

DynGFN: Bayesian Dynamic Causal Discovery using Generative Flow Networks

Lazar Atanackovic^{*12} Alexander Tong^{*34} Jason Hartford³⁴ Leo J. Lee¹² Bo Wang¹²⁵ Yoshua Bengio³⁴⁶

Abstract

Learning the causal structure of observable variables is a central focus for scientific discovery. Bayesian causal discovery methods tackle this problem by learning a posterior over the set of admissible graphs given our priors and observations. Existing methods primarily consider observations from static systems and assume the underlying causal structure takes the form of a directed acyclic graph (DAG). In settings with dynamic feedback mechanisms that regulate the trajectories of individual variables, this acyclicity assumption fails unless we account for time. We focus on learning Bayesian posteriors over cyclic graphs and treat causal discovery as a problem of sparse identification of a dynamical system. This imposes a natural temporal causal order between variables and captures cyclic feedback loops through time. Under this lens, we propose a new framework for Bayesian causal discovery for dynamical systems and present a novel generative flow network architecture (DynGFN) tailored for this task. Our results indicate that DynGFN learns posteriors that better encapsulate the distributions over admissible cyclic causal structures compared to counterpart state-of-the-art approaches.

1. Introduction

The first step to understanding a complex system is to understand the dependencies between its variables. Because of this, accurately modelling the causal dependencies between observable variables is a focal point for progress in scientific discovery. Causal discovery methods aim to automate this task by learning the graph that relates these variables (Glymour et al., 2019; Pearl, 2009; Peters et al., 2017). Most methods have focused on fully observed static

systems where the true graph is assumed to be directed and acyclic (i.e. the graph is a “DAG”), which enables structure learning (up to Markov equivalence classes) because conditional independence among variables imply missing edges in the causal graph. However, many natural systems are dynamic in nature with complex time varying behavior and feedback loops that induce cyclicity in the time-collapsed graph (“the summary graph”) (Peters et al., 2022). Hence, considering only static data rules out most causal structure learning approaches. In this work, we consider the problem of modelling epistemic uncertainty over dynamic causal structure from finite time-series data. At its root, this problem requires structure learning over cyclic graphs which poses an extra challenge for current state-of-the-art causal discovery methods.

Causal events naturally proceed through time: if y is a cause of x , then the effect on x must precede the observed effects on y (Granger, 1969). Therefore, we aim to leverage time-series observations to identify the causal structure between variables that define the data generating process of a dynamical system. Dynamical system models are a natural tool of choice when trying to capture dependencies between variables with time-series data. From a dynamical systems perspective, one can model both causal structure between variables as well as their time-dependent system response with the drift function (Mooij et al., 2013; Peters et al., 2022), and hence we can treat causal discovery as a problem of identification of a dynamical system. However, jointly identifying the sparse causal structure between variables and their respective dynamic relationships is a persisting challenge.

There is a lot of prior work on the problem of identifying causal structure G from either observational (e.g. Spirtes & Glymour, 1991; Zheng et al., 2018; Monti et al., 2020) or interventional (e.g. Ke et al., 2019; Lachapelle et al., 2020; Mooij et al., 2020) data but the majority of existing methods return only the most likely directed acyclic graph under the observed data. In many scientific settings it is prohibitively expensive to acquire a sufficient quantity of data with low measurement noise, so in finite samples there may be a large set of candidate graphs that are consistent with the observed data. Capturing this uncertainty is critical for downstream

^{*}Equal contribution ¹University of Toronto ²Vector Institute ³Mila - The Quebec AI Institute ⁴Université de Montréal ⁵University Health Network ⁶CIFAR Fellow. Correspondence to: Lazar Atanackovic <l.atanackovic@mail.utoronto.ca>.

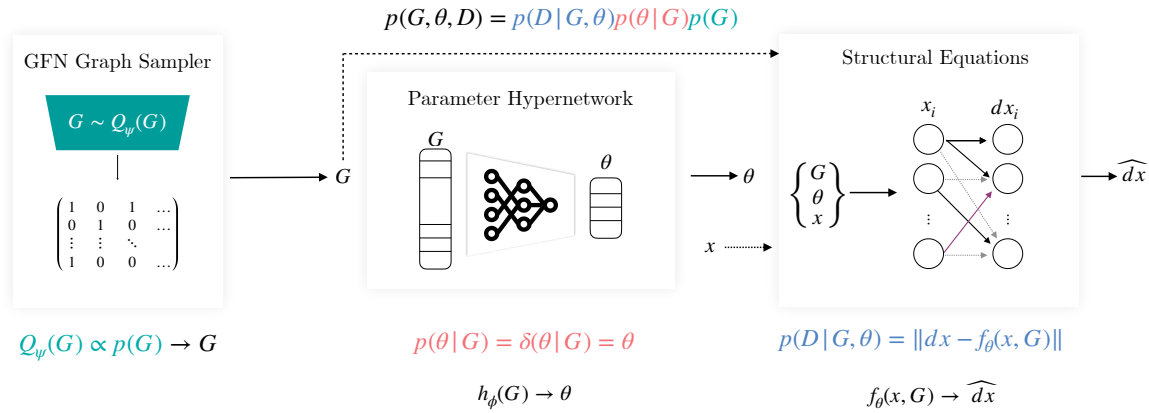


Figure 1. Architecture for Bayesian causal discovery of dynamical systems. DynGFN consists of three main components: A GFlowNet modeling a posterior distribution over graphs $Q(G|D)$, a hyper network modeling a posterior over parameters given a graph $Q(\theta|G, D)$, and the structural equation model scoring G and θ according to how well they fit the data. Although the figure shows the case where $Q(G|D)$ is modelled with a GFlowNet, this can be any arbitrary graph sampler that can sample discrete structures $G \sim Q(G|D)$.

scientific applications.

Bayesian causal discovery methods address this by modelling a posterior over admissible directed acyclic graph (DAG) structures $P(G|D)$ that explain the observational data (Lorch et al., 2021; Cundy et al., 2021; Annadani et al., 2021; Deleu et al., 2022; Lopez et al., 2022). Recently, applications of Generative Flow Networks (GFlowNets) have shown success for modelling $P(G|D)$ (Deleu et al., 2022). GFlowNets (Bengio et al., 2021; 2022) parameterize the distribution over graphs (or any discrete object) through a sequential policy, and as a result avoid needing to make restrictive parametric assumptions on the distribution over admissible graphs. This makes them a useful tool in structure discovery, however it remains restrictive to assume the underlying causal structure of the observed system is a DAG as natural dynamic systems typically contain feedback loops.

To tackle the problem of Bayesian dynamic causal discovery, we devise a framework of two key components. First, we learn a graph sampler $Q(G)$ that models posterior $P(G|D)$ over cyclic graphs. We then use graphs samples from $Q(G)$ unrolled over time to learn a directed structural causal model (SCM). We consider flexible parameterizations for the SCM capturing both linear and non-linear dynamic relationships. Since $P(G|D)$ is a discrete distribution, we propose to use of GFlowNets to learn $Q(G)$ and show a use-case of our framework for causal discovery of gene regulatory networks (GRNs). Our main contributions are summarized as follows:

- We develop a novel framework for Bayesian causal discovery under the lens of dynamical system identification for modelling posteriors over cyclic graphs. In ad-

dition, we apply existing state-of-the art DAG Bayesian structure learning approaches under our framework to learn cyclic graphical structure.

- We design a novel GFlowNet architecture (DynGFN) tailored for modelling posteriors over temporal causal graphs. We additionally leverage a per-node factorization within DynGFN that enables efficient search over the discrete space of cyclic graphs for systems of moderate size.
- To test learning of Bayesian posteriors over structures we empirically evaluated DynGFN on synthetic dynamic data designed to induce highly multi-modal posteriors over causal graphs. Using single-cell RNA-velocity data we demonstrate an application of our framework for learning posteriors of gene regulatory networks.

While we show a specific use-case for discovery of GRNs, our framework is applicable to a broad range of problems where a system is dynamic in nature and can be observed over time.

2. Related Work

Recently, there has been significant interest in fully differentiable Bayesian methods for causal discovery in the static case. DiBS (Lorch et al., 2021), BCD-Nets (Cundy et al., 2021), VCN (Annadani et al., 2021), and DAG-GFlowNet (Deleu et al., 2022) all attempt to learn a distribution over causal models from a fully observed system. The key difference is in how these methods parameterize the

graph. DiBS is a particle variational inference method that uses two matrices U and V where $G = \text{sigmoid}(U^T V)$ where the sigmoid is applied elementwise which is similar to graph autoencoders. BCD-Nets and DP-DAG use the Gumbel-Sinkhorn distribution to parameterize a permutation and direct parameterization of a lower triangular matrix. VCN uses an autoregressive LSTM to generate the graph as this gets rid of the standard unimodal constraint of Gaussian distributed parameters. In small graphs, these methods can model the uncertainty over possible models (including over Markov equivalence classes). However, there has been comparatively little work towards Bayesian structure learning from dynamics. Recent works in this direction based on NeuralODEs (Chen et al., 2018) propose a single explanatory structure (Tank et al., 2021; Bellot & Branson, 2022; Aliee et al., 2021), but do not attempt to model uncertainty over the explanatory structure. Motivated by gene regulatory networks, in this work our goal is to model uncertainty over the explanatory graph for a dynamical system.

One dynamical system of interest is that of cells. Cellular response to environmental stimuli or genetic perturbations can be modelled as a complex time-varying dynamical system (Hashimoto et al., 2016; Aliee et al., 2021). In general, dynamical system models are a useful tool for downstream scientific reasoning. In this work we are primarily interested in identifying the underlying cell dynamics from data. A reasonable model for cell dynamics is as a stochastic dynamical system with many, possibly unobserved, components. There are many data collection models for gaining insight into this system from single-cell RNA-sequencing data. We will primarily focus on RNA velocity type methods, where both x and an estimate of dx are available in each cell, but note that there are other assumptions to infer dynamics and regulation such as pseudotime-based methods (Saelens et al., 2019; Aliee et al., 2021), and optimal transport methods (Hashimoto et al., 2016; Schiebinger et al., 2019; Tong et al., 2020; Huguet et al., 2022a;b). After learning a possible explanatory regulation, this is used in downstream tasks, but the resulting conclusions drawn from these models are necessarily conditional on the inferred regulation. In DynGFN, we instead explicitly model uncertainty graphs which allows us to propagate the resulting uncertainty to downstream conclusions.

3. Preliminaries

3.1. A Structural Model for Dynamical Systems

A structural causal model (SCM) describes the structured relationships between a set of random variables x_1, x_2, \dots, x_d encoded by a DAG \mathcal{G} with d vertices: $x_i = f_i(\text{Pa}(x_i), \epsilon_i)$. Here, $\text{Pa}(x_i)$ denotes the parents of x_i and ϵ_i are mutually independent noise terms. If we observe a time-series $x = (x_1, x_2, \dots, x_d) : [0, T] \rightarrow \mathbb{R}^d$ we can define the par-

ents, $\text{Pa}(x_i)$, as previous temporal instances of x_i and define a dynamic structural model (Mooij et al., 2013; Peters et al., 2022) of the form

$$\frac{dx_i(t)}{dt} = f_i(x, \epsilon_i). \quad (1)$$

In this work, we consider a setting where we observe n dynamic pairs $(x, dx) \in \mathbb{R}^d \times \mathbb{R}^d$, and learn a parameterized function $f_\theta(x, \epsilon) : \mathbb{R}^d \rightarrow \mathbb{R}^d$ that approximates the structural model defined in (1).

3.2. Bayesian Structure Discovery

We consider finite data \mathcal{D} in \mathbb{R}^d sampled noisily from an underlying stochastic dynamical system governed by a latent drift $\frac{dx}{dt} = f(x)$ which has some sparsity pattern i.e. $\frac{\partial f_i}{\partial x_j} \neq 0$ for a small set of variables, which can be parameterized by a graph G such that $G_{ij} = \mathbf{1}[\frac{\partial f_i}{\partial x_j} \neq 0]$. Furthermore, we do not directly observe x , but rather observe $y \sim x + \epsilon$ where ϵ is independent noise. We would like to model our posterior over explanatory graphs given the data $Q(G|\mathcal{D})$. We assume a generative model with the following factorization:

$$p(G, \Theta, \mathcal{D}) = p(G)p(\Theta|G)p(\mathcal{D}|G, \Theta) \quad (2)$$

This factorization forms the basis of our inference procedure.

3.3. Generative Flow Networks

GFlowNets are an approach for learning generative models over spaces of discrete objects (Bengio et al., 2021; 2022). GFlowNets learn a stochastic policy $P_F(\tau)$ to sequentially sample an object \mathbf{x} from a discrete space \mathcal{X} . Here $\tau = (s_0, s_1, \dots, s_n)$ represents a full Markovian trajectory over plausible discrete states, where s_n is the terminating state (i.e. end of a trajectory) (Malkin et al., 2022). The GFlowNet is trained such that at convergence, sequential samples from the stochastic policy over a trajectory, $\mathbf{x} \sim P_F(\tau)$, are equal in distribution to samples from the normalized reward distribution $P(x) = \frac{R(\mathbf{x})}{\sum_{\mathbf{x}' \in \mathcal{X}} R(\mathbf{x}')}.$

The GFlowNet policies are typically trained by optimizing either the *Trajectory Balance* (Malkin et al., 2022) or the *Detailed Balance* (Deleu et al., 2022) loss.

Trajectory Balance Loss: For a complete trajectory τ , the trajectory balance (TB) loss is defined as:

$$\mathcal{L}_{\text{TB}}(\tau) = \left(\log \frac{Z_\psi \prod_{i=1}^n P_F(s_i | s_{i-1}; \psi)}{R(x) \prod_{i=1}^n P_B(s_{i-1} | s_i; \psi)} \right)^2, \quad (3)$$

where $P_F(s_i | s_{i-1}; \psi)$, $P_B(s_{i-1} | s_i; \psi)$, and Z_ψ represent the forward transition probability, backward transition probability, and a trainable normalizing constant, respectively.

The TB loss in (3) requires full trajectories τ , which may cause challenges when scaling to larger discrete search spaces due to increased variance of gradients when training of the stochastic policy (Malkin et al., 2022).

Detailed Balance Loss: The detailed balance (DB) loss (Deleu et al., 2022) leverages the fact that the reward function can be evaluated for any partially constructed graph (i.e. any prefix of τ), and hence we get intermediate reward signals for training the GFlowNet policy. The DB loss is defined as:

$$\mathcal{L}_{\text{DB}}(s_i, s_{i-1}) = \left(\log \frac{R(s_i)P_B(s_{i-1}|s_i;\psi)P_F(s_n|s_{i-1};\psi)}{R(s_{i-1})P_F(s_i|s_{i-1};\psi)P_F(s_n|s_i;\psi)} \right)^2. \quad (4)$$

Under this formulation, during GFlowNet training the reward is evaluated at every state. This differs from the TB loss where the reward is only computed once a complete trajectory is sampled. For this reason, the DB formulation is in general advantageous for the structure learning problem where any sampled graph can be viewed as a complete state, hence more robustly inform gradients when training the stochastic policy. Previous work has shown GFlowNets are useful in settings with multi-modal posteriors. This is of particular interest to us where many admissible structures can explain the observed data equally well.

3.4. Learning Gene Regulatory Networks from Single-cell Data

Single-cell transcriptomics has an interesting property in that from a single measurement we can estimate both the current state x and the current velocity dx . Because mechanistically RNA undergoes a splicing process, we can measure the quantities of both the unspliced (early) and spliced (late) RNA in the cell. From these two quantities we can estimate the current RNA content for each gene and the current transcription rate. There exist many models for denoising and interpreting this data (La Manno et al., 2018; Bergen et al., 2019; Qiu et al., 2022). Furthermore, there exist more elaborate measurement techniques to extract more accurate velocity estimates (Qiu et al., 2022). The fact that we have an estimate of the current velocity is exceptionally useful for continuous time structure discovery because it allows us to avoid explicitly unrolling the dynamical system.

Learning the underlying causal structure from data is one of the open problems in biology. There are many works that attempt to learn the effect of a change in a gene, or the addition of a drug. These works often build models that directly predict the outcome of an intervention. This may be useful for certain applications, but often does not generalize well out of distribution. We would like to learn a model of the underlying instantaneous dynamics that give

rise to effects at longer time scales. This approach has a number of advantages. (1) it is closer to the mechanistic model; it may be easier to learn a model of the instantaneous dynamics rather than the dynamics over long time scales. (2) One model can be trained and applied to data from many sources including RNA-velocity, Pseudotime, Single-cell time series, and steady state perturbational data. (3) The instantaneous graph may be significantly sparser (and therefore easier to learn) than the summary graph or the equilibrium graph.

4. DynGFN for Bayesian Dynamic Causal Discovery

We present a general framework for Bayesian dynamic causal discovery and propose a GFlowNet architecture, DynGFN, tailored for modelling a posterior over discrete graphical structures. We summarize our framework in Figure 1 and Algorithm 1. DynGFN consists of 3 key modules:

1. A graph sampler that samples graphical structures that encode the causal dependencies among the observed variables. This is parameterized with a GFlowNet that iteratively adds edges to a graph.
2. A class of structural equation modules that models the functional relationships between the observed variables, indexed by parameters θ . This is a class of functions that respect the conditional independencies implied by the graph sampled in step 1. We enforce this by masking inputs according to the graph.
3. Because the functional relationships between variables may be different depending on which graph is sampled, we rely on a hyper network architecture that outputs the parameters θ of the structural equations as a function of the graph.

For training, we assume L^0 sparsity of graphs G to constrain the large discrete search space over possible cyclic structures. The main advantage of DynGFN comes when modelling posteriors with many modes. Prior work has shown GFlowNets are able to efficiently model distributions where we can share information between different modes (Malkin et al., 2022). The challenge we tackle is how to do this with a changing objective function, as the GFlowNet objective is a function of the current parameter hyper network and the structural equations.

4.1. Graph Sampler

DynGFN models a posterior distribution over graphs $Q(G|D)$ given a finite set of observations. To learn $Q(G|D)$, DynGFN needs to explore over a large discrete state space. Since we aim to learn cyclic graphs, DynGFN

Algorithm 1 Batch update training of DynGFN with detailed balance loss

```

1: Input: Data batch  $(x_b, dx_b)$ , initial NN weights  $\psi, \phi$ ,
    $L^0$  sparsity prior  $\lambda_0$ , and learning rate  $\epsilon$ .
2:  $s_0 \leftarrow \mathbf{0}_{B \times d \times d} \triangleright$  Training is paralleled over  $B$  graph
   trajectories
3:  $a \sim P_F(s_1|s_0; \psi)$ ,  $\triangleright$  Sample initial actions vector
4: while  $a$  not  $\emptyset$  do
5:   Compute  $P_F(s_i|s_{i-1}; \psi)$ ,  $P_B(s_{i-1}|s_i; \psi)$ 
6:    $\theta \leftarrow h_\phi(s_i)$ 
7:    $\widehat{dx}_b \leftarrow f_\theta(x, s_i)$ 
8:    $R_i(s_i) \leftarrow e^{-\|dx_b - \widehat{dx}_b\|_2^2 + \lambda_0 \|s_i\|_0}$ 
9:    $\psi \leftarrow \psi - \epsilon \nabla_\psi \mathcal{L}_{DB}(s_i, s_{i-1}) \triangleright \mathcal{L}_{DB}(s_i, s_{i-1})$ 
   computed as in Equation 4
10:   $a \sim P_F(s_i|s_{i-1}; \psi)$ ,  $s_i \rightarrow s_{i+1} \triangleright$  Take action step
   to go to next state
11:  $\phi \leftarrow \phi - \epsilon \nabla_\phi \log R$ 
   return Updated GFN weights  $\psi$  and updated hyper
   network weights  $\phi$ .
    
```

needs to search over 2^{d^2} possible structures, where d denotes the dimensionality of the system and d^2 the number of possible edges in G . For even moderate d , this discrete space is very large (e.g. for $d = 20$ we have 2^{400} possible graphs).

However, if we are willing to assume independence between the outputs of our model, then we can greatly reduce this search space, that is that $Q(G|D)$ factorizes. This is not an entirely unreasonable assumption, and is fulfilled if the structural equations are linear. In this case we factorize $Q(G|D)$ by node as

$$Q(G|D) = \prod_{i \in [1, \dots, d]} Q_i(G[i, \cdot] | D) \quad (5)$$

By using this model, we reduce the search space from $2^{d^2} \rightarrow d2^d$. For $d = 20$ this is $\approx 2^{104}$. While still intractable to search over, it is still a vast improvement over the unfactorized case. We call this model a *per-node* posterior, and we use a per-node GFlowNet going forward.

4.2. Hyper Network and Structural Model

We aim to jointly learn the structural encoding G and parameters θ that together model the causal relationships $dx = f_\theta(x, G)$ of the dynamical system variables. To accomplish this, we propose learning an individual set of parameters θ for each graph G and independent of the input data x . This approach encapsulates $P(\theta|G)$ in (2). We use a hyper network architecture that takes G as input and outputs the structural equation model parameters θ , i.e. $\theta = h_\phi(G)$ hence $P(\theta|G) = \delta(\theta|G)$. This hyper network model does not capture uncertainty in the parameters, however the for-

mulation may be extended to the Bayesian setting by placing a prior on the hyper network parameters ϕ . Although h_ϕ allows for expressive parameterizations for θ , it may not be easy to learn¹.

Linear Assumption on Dynamic Structural Model: In addition to analytically modelling linear systems, in some cases it may suffice to assume a linear differential form $\frac{dx}{dt} = Ax$ to approximate dynamics. In this setting, given a sampled graph $G \sim Q(G)$ and n observations of (x, dx) we can solve for $\theta = A$ analytically. To induce dependence on the graph structure, we use the sampled G as a mask on x and construct $\tilde{x}_i = G_i^T \odot x$. Then we can solve for θ on a per-node basis as

$$\theta_i = (\tilde{x}_i^T \tilde{x}_i + \lambda I)^{-1} \tilde{x}_i^T dx_i, \quad (6)$$

where $i = 1, \dots, d$, $\lambda > 0$ is a hyper-parameter, and I is the identity matrix.

4.3. GFlowNet Exploration vs. Exploitation

The general procedure for training GFlowNets is inspired from reinforcement learning where the primary objective is to learn a stochastic policy $\pi(a|s)$ to sample actions from an action space given a current state. In our setting, the action space represents possible locations where an additional edge can be placed to an existing graph and each state is represented by a current graph. Since under this training procedure we are sampling from the GFlowNet policy $P_F(s_i|s_{i-1}; \psi)$ at every iteration then attributing a reward associated to the sampled state/graph, the policy is susceptible to exploitation: if $P_F(s_i|s_{i-1}; \psi)$ samples a graph(s) with a high reward, it becomes easy for the policy to focus on sampling said graphs since they yield high reward. To alleviate this we encourage exploration using softmax tempering on our stochastic policy, by multiplying the logits of our forward policy by $1/c$ before applying the softmax function. A larger c flattens the stochastic policy such that exploration within the action space is encouraged. However, setting the parameters c is challenging and there exists a trade-off between exploring and exploiting the stochastic policy during optimization. We address this by using a cosine schedule for c such that $1 \leq c \leq 1000$. We treat the period of the cosine schedule as a hyper-parameter.

5. A Useful Model of Indeterminacy

In order to evaluate DynGFN, we need a structure learning problem with a large equivalence class of admissible graphs. We present a simple way to augment a set of identifiable dynamics under some model to create a combinatorial number of equally likely dynamics under the same model. More specifically, this creates a ground truth pos-

¹We discuss training dynamics when using h_ϕ in section 6.5.

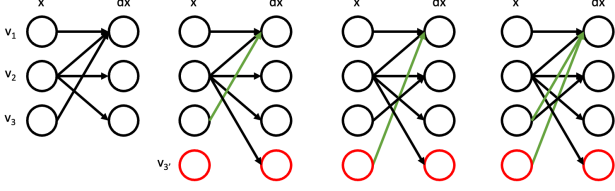


Figure 2. For an identifiable graph, we add a new variable which has the same values as v_3 and creates three possible explanations for the data (green). If we consider a sparsity penalty, then we can eliminate the last possibility for only two possible explanations.

terior $Q^*(G|D) \propto \sum T(G^*)$ where $T(\cdot) : \mathcal{G} \rightarrow \mathcal{G}$ is an analytically computable transformation over graphs and G^* is the identified graph under the original dynamics. We use this system to test how well we can learn a posterior over structures that matches what we see in single-cell data.

Specifically, given a dataset of $(x, dx) \in \mathbb{R}^d \times \mathbb{R}^d$ pairs, we create a new dataset with $d + 1$ variables where the ‘new’ variable v' is perfectly correlated with an existing variable v . In causal terms, this new variable inherits the same parents as v , that is $\text{Pa}(v') := \text{Pa}(v)$ and the same structural equations as v , that is $dv' = dv$. This is depicted in Figure 2. This creates a number of new possible explanatory graphs, which we generalize with the following proposition.

Proposition 1. *Given any d dimensional ODE system with G^* identifiable under $f \in \mathcal{F}$, the $D = d + a$ dimensional system $\frac{dx}{dt} = Ax$, denote the vector of multiplicities $m \in \mathbb{N}^d$ with m_i as the number of repetitions of each variable. Then this construction creates an admissible family of graphs \mathcal{G}' where $|\mathcal{G}'| = \prod_{i \in d} (2^{m_i} - 1)^{\mathcal{G}_i^1}$. Furthermore, under an L^0 penalty on G , this reduces to $\prod_i (m_i)^{\mathcal{G}_i^1}$.*

See Sec. A for full proof. The intuition behind this proposition can be seen from the case of adding a single copied variable. This corresponds to $A = [\delta_v I_d]$ where δ_v is a vector with a 1 on node v and zeros elsewhere, and I_d is the d -dimensional identity matrix. Let v have c children, such that $v \in \text{Pa}(c)$ in the identifiable system, then any of those c child nodes could depend either on v or on the new node v' or both. This creates 3^c possible explanatory graphs. If we restrict ourselves to the set of graphs with minimal L^0 norm, then we eliminate the possibility of a child node depending on both v and v' , this gives 2^c possible graphs, choosing either v or v' as a parent.

6. Experimental Results

In this section we evaluate the performance of DynGFN against other methods for Bayesian structure learning. We show in certain cases, DynGFN is able to better capture the true posterior when there are a large number of modes. We evaluate methods according to three metrics, Bayes-SHD,

Table 1. Bayesian dynamic causal discovery of linear and non-linear systems with $d = 20$ variables (i.e. discovery over 20×20 graphs). The graphs representing the causal dynamic relationships of the linear and non-linear systems have 50 edges out of possible 400. The ground truth discrete distribution $P(G^*)$ contains 1024 admissible graphs for each respective system. The ℓ and h pre-fix denote usage of the analytic linear solver and hyper-network solver for SCM parameters, respectively. Results are reported on held out test data over 5 model seeds.

Linear System			
Model	Bayes-SHD ↓	AUC ↑	KL ↓
ℓ -DynBCD	32.0 ± 0.27	0.71 ± 0.0	1694.74 ± 9.17
ℓ -DynDiBS	29.2 ± 0.78	0.71 ± 0.0	6388.85 ± 135.84
ℓ -DynGFN	22.8 ± 1.41	0.75 ± 0.01	1117.5 ± 20.63
h -DynBCD	134.5 ± 89.40	0.64 ± 0.17	2212.7 ± 50.51
h -DynDiBS	32.9 ± 10.40	0.50 ± 0.07	6366.63 ± 3414.81
h -DynGFN	24.1 ± 3.40	0.76 ± 0.02	26504.0 ± 4474.88

Non-linear System			
Model	Bayes-SHD ↓	AUC ↑	KL ↓
ℓ -DynBCD	78.1 ± 7.32	0.42 ± 0.03	3171.84 ± 97.72
ℓ -DynDiBS	75.3 ± 7.30	0.59 ± 0.01	6131.15 ± 53.34
ℓ -DynGFN	45.7 ± 0.62	0.55 ± 0.0	234.8 ± 3.60
h -DynBCD	194.0 ± 0.25	0.50 ± 0.0	2405.98 ± 428.78
h -DynDiBS	45.3 ± 6.39	0.51 ± 0.09	8795.00 ± 145.58
h -DynGFN	38.9 ± 7.45	0.69 ± 0.02	4878.57 ± 659.77

area under the receiver operator characteristic curve (AUC), and Kullback–Leibler (KL) divergence between learned posteriors $Q(G)$ and the distribution over true graphs $P(G^*)$. These metrics can only be evaluated when we have a ground truth posterior over over structures. Bayes-SHD measures the average distance to the closest structure in the admissible set of graphs according to the structural hamming distance, which in this case is simply the hamming distance of the adjacency matrix representation to the closest admissible graph.

6.1. Baselines for Bayesian Dynamic Causal discovery

Existing Bayesian structure learning methods are typically constrained to learning DAGs. Temporal information about the the dynamic relationships amongst variables in a system can help alleviate this constraint. DiBS and BCD-Nets are two state-of-the-art Bayesian causal discovery approaches for static systems. We apply versions of DiBS and BCD-Nets such that they are applicable in our Bayesian dynamic causal discovery framework for learning cyclic causal structure from dynamic data. We use the approach taken in DiBS and parameterize the distribution over graphs as $P_{\alpha_t}(G|Z) = \prod_i \prod_j P_{\alpha_t}(G_{ij}|Z_{ij})$, where $Z = U^T V$, $U, V \in \mathbb{R}^{k \times d}$. Here $P_{\alpha_t}(G_{ij} = 1|Z_{ij}) = \sigma(\alpha_t Z_{ij})$, $\sigma(x) = 1/(1 + e^{-\alpha_t x})$, and $\alpha_t = \alpha c(t)$ (t denotes the training iteration. We use $c(t) = \sqrt{t}$). As $t \rightarrow \infty$, $P_{\alpha_t}(G|Z) \rightarrow \delta(G|Z)$. In DiBS, Stein variational gradi-

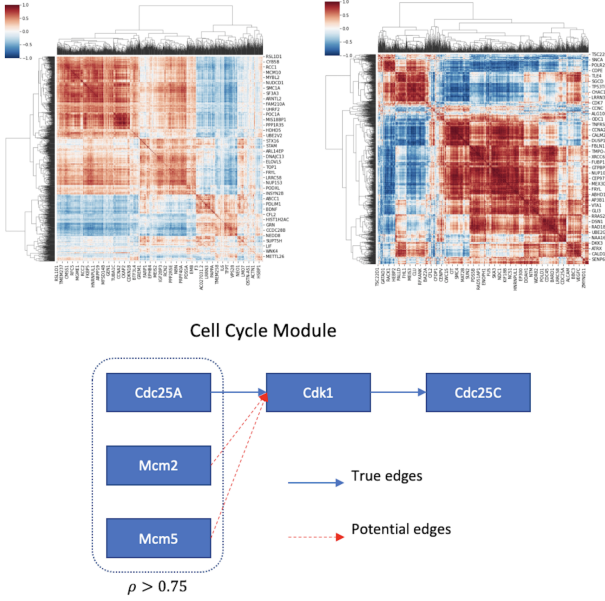


Figure 3. From left to right, correlation structure in the raw single cell data over 5000 cells and 2000 genes selected by scVelo (Bergen et al., 2019) preprocessing. Correlation structure among genes over (inferred) cell cycle times. This stronger correlation structure is more reflective of the correlation in the underlying system. Cdc25A is known to inhibit Cdk1 which is known to inhibit Cdc25C, while the Mcm complex is highly correlated with Cdc25A, they do not directly interact with Cdk1 (Kanehisa et al., 2021).

ent decent (SVGD) (Liu & Wang, 2016) is used to iteratively transport particles Z to learn the target distribution. Following from the above parameterization, we implement BCD-Nets by treating $U \sim \mathcal{N}(\mu_u, \sigma_u^2)$, $V \sim \mathcal{N}(\mu_v, \sigma_v^2)$, and learning μ_u, μ_v, σ_u , and σ_v . Since our framework uses dynamic data, we incorporate DiBS and BCD-Nets within the framework (labeled DynDiBS and DynBCD, respectively) to leverage dynamic information for causal discovery of cyclic graphs.

6.2. Toy Examples with Known Posteriors

We generated toy unidentifiable data from two systems using our indeterminacy model presented in section 5: (1) a linear dynamical system $dx = Ax$, and (2) a non-linear dynamical system $dx = \text{sigmoid}(Ax)$. We consider ℓ -DynGFN and h -DynGFN, DynGFN with linear analytic parameter solver as shown in equation (6), and DynGFN with the hyper-network parameter solver h_ϕ . Likewise, we compare ℓ -DynGFN and h -DynGFN to counter part baselines we call ℓ -DynBCD, ℓ -DynDiBS, h -DynBCD, and h -DynDiBS. To constrain the discrete search procedure, we assume a sparse prior on the structure the graphs G , specifically the L^0 prior. Due to challenging iterative optimization dynamics present

Table 2. Ablation for ℓ -DynGFN on $d = 20$ systems with various levels of sparsity. Here sparsity is a dynamic data generation parameter that control the number of edges in the ground truth graphs. For a sparsity level of 0.9, the ground truth graphs have 50 edges out of d^2 possible edges. In this experiment, the true $P(G)$ has 1024 modes. We conduct this ablation over 5 random seeds.

Sparsity	Bayes-SHD \downarrow	AUC \uparrow	KL \downarrow
0.95	16.4 ± 1.71	0.79 ± 0.0	889.57 ± 31.24
0.90	22.8 ± 1.41	0.75 ± 0.01	1117.5 ± 20.63
0.85	32.8 ± 0.72	0.71 ± 0.0	—
0.80	39.2 ± 0.69	0.71 ± 0.0	—
0.75	60.2 ± 1.17	0.66 ± 0.01	—

when using $\theta = h_\phi(G)$ for DynGDN, to train initialize the forward policy $P_F(s_i|s_{i-1}; \psi)$ using the ψ learned in ℓ -DynGFN to provide a more admissible starting point for learning h_ϕ (we discuss further details in section 6.5). We do not need to do this for h -DynBCD and h -DynDiBS as we are able to train both models end-to-end without iterative optimization.

In Table 1 we show results of our synthetic experiments for learning posteriors over multi-modal distributions of cyclic graphs. We observe the ℓ -DynGFN is most competitive on the linear system across all three metrics. When in the hyper-network regime on the linear system, h -DynGFN outperforms h -DynDiBS and h -DynBCD on Bayes-SHD and AUC, however h -DynBCD is most competitive with respect to KL. On the non-linear system, ℓ -DynGFN outperforms counterpart methods in terms of KL. We observe that although h -DynGFN improves upon Bayes-SHD, it yields a higher KL. Details about DynGFN, baselines, and accompanying hyperparameters can be found in Appendix B.

6.3. Ablation over Sparsity of Dynamic System

Identifying admissible causal structure from observational data is a challenging problem. Consequently, DynGFN and corresponding methods rely on the use of priors to effectively learn causal structure, e.g. sparsity of graphs. Because of this, we use the L^0 prior on G throughout training. Under this setting, system sparsity carries significant weight on the ability to learn posteriors over the causal dynamics of a system. In Table 2 we show this behaviour empirically through an ablation study. We note that computing the KL-divergence for DynGFN, specifically computing the probability generating a true G , becomes computationally intractable as G is less sparse². For systems of 0.9 and

²For example, since DynGFN constructs one object G sequentially over a state space distribution, we must compute probabilities of all combinatorial state trajectories for constructing $G = (s_i, \dots, s_n)$. The space of combinatorial state trajectories is $n!$ factorial in nature, hence this computation is only possible for small graphs and/or sparse graphs.

Table 3. Bayesian dynamic causal discovery 5-D cellular system using scRNA velocity data. The dynamics of this system are unknowns, however we identify 81 admissible graphs between variables (genes) that describe the data. We train models over 5 seeds. The graphs of this system contain of 7 true edges.

Model	Cellular System - RNA Velocity		
	Bayes-SHD ↓	AUC ↑	KL ↓
ℓ -DynBCD	2.57 ± 0.08	0.56 ± 0.01	301.74 ± 2.15
ℓ -DynDiBS	5.77 ± 0.36	0.45 ± 0.01	554.20 ± 28.44
ℓ -DynGFN	3.11 ± 0.17	0.57 ± 0.00	74.49 ± 6.77
h -DynBCD	10.11 ± 0.75	0.53 ± 0.03	46.08 ± 3.91
h -DynDiBS	9.07 ± 4.73	0.62 ± 0.10	511.61 ± 118.84
h -DynGFN	6.05 ± 0.55	0.56 ± 0.03	19.49 ± 9.00

0.95 sparsity, we observe a decreasing trend in KL and Bayes-SHD, while an increasing trend in AUC. This result is expected as DynGFN can better traverse sparse graphs as the combinatorial space over possible trajectories is smaller relative to denser systems.

6.4. Single-Cell RNA-velocity Data

To show how this can be applied to single cell data we use a cell cycle dataset of human Fibroblasts. The process of Eukaryotic cell division can be divided into four well regulated stages based on the phenotype, Gap 1 (G_1), Synthesis (S), Gap 2 (G_2), and Mitosis (M). This process is a good starting point for GRN discovery as it is (1) relatively well understood, (2) deterministic, and (3) well studied with plentiful data. While there is an underlying control loop controlling the progression of the cell cycle, there are many other genes that also change during this cycle. To rediscover the true control process from data we must disentangle the true causal genes from the downstream correlated genes. This may become very difficult when we only observe dynamics at longer time scales.

As a motivating example we show the correlation structure of single-cell RNA-seq data from human Fibroblast cells (Riba et al., 2022) in Figure 3. We show both the raw correlation and the correlation over cell cycle time, which is significantly higher. With such a pure cell population whose primary axis of variation is state in the cell cycle by aggregating over cell cycle time we expect observation noise to be averaged out, leading to a “truer” view of the correlation between latent variables.

Since there are many genes which are affected by the cell cycle phase, there are many correlated variables that are downstream of the true cell cycle regulators. This provides a natural way of using cell cycle data to evaluate a model’s ability to capture the Bayesian posterior. We hide a cell cycle regulator among two downstream genes that are highly correlated (Spearman $\rho > 0.75$) and test whether we can model the Bayesian posterior – namely that we are uncertain

about which of the three genes (Cdc25A, Mcm2, or Mcm5) is the true causal parent of Cdk1.

In Table 3 we show results for a learning posteriors over a undetermined GRN using RNA velocity data. We find that ℓ -DynGFN and h -DynGFN yield low KL and moderate Bayes-SHD. While ℓ -DynBCD performs well in terms of identify a small distribution of true G ’s, it falls short in modelling the true posterior (this can be seen from low Bayes-SHD, high KL).

6.5. Discussion of Training Dynamics

GFlowNets are a relatively recent class of models that can be challenging to optimize. We discuss some of the challenges with training them especially in the context of a learned energy function. We observed that in settings where the energy reward is fixed and we could proportionally penalize missing edges as well as the addition of incorrect edges (e.g. ℓ -DynGFN), we were able to better learn posteriors over admissible graphs over models that require sparse priors and/or trainable energies. This suggests that DynGFN may be limited by an inadequate energy reward. However, we found training DynGFN with a trainable energy function challenging since the GFlowNet stochastic policy depends on the rewards, and vice versa. Further investigation and experimentation into this alternating optimization procedure is required.

7. Conclusion

We presented DynGFN, a method for Bayesian causal discovery from dynamics. In low dimensions we found that DynGFN is able to better model the distribution over possible explanatory structures than baseline methods. As a proof of concept, we presented an example of learning the distribution over likely explanatory graphs from single-cell transcriptomic data where there are many possible graphs, showing DynGFN can better model the uncertainty over possible explanations of this data rather than capturing a single explanation. Although we have demonstrated a degree of efficacy when using DynGFN for Bayesian causal discovery with observational data, a key limitation of DynGFN is scaling to larger systems. To effectively model $P(G, \theta, D)$, DynGFN needs to search over an environment state space of possible graphs. This state space grows exponentially with the number of possible edges, i.e. 2^{d^2} or d^{2d} for per-node-GFN where d is the number of variables in the system. Therefore, DynGFN is currently limited to smaller systems. We also found that training DynGFN requires careful tuning of hyper-parameters and in particular parameters that shape the reward function are particularly important. Nevertheless, there are many applications where Bayesian causal discovery even over 5-20 dimensional examples we explore here could be extraordinarily useful.

ACKNOWLEDGMENTS

The authors acknowledge funding from the Natural Sciences and Engineering Research Council of Canada (NSERC), Recursion Pharmaceuticals, CIFAR, Genentech, Samsung and IBM. This research was enabled in part by the computational researches provided by Compute Canada ([ccdb.compute.canada.ca](https://compute.canada.ca)). In addition, resources used in preparing this research were in part provided by the Province of Ontario and companies sponsoring the Vector Institute (vectorinstitute.ai/partners/).

References

- Aliee, H., Theis, F. J., and Kilbertus, N. Beyond predictions in neural odes: Identification and interventions. *arXiv preprint 2106.12430*, 2021.
- Annadani, Y., Rothfuss, J., Lacoste, A., Scherrer, N., Goyal, A., Bengio, Y., and Bauer, S. Variational causal networks: Approximate bayesian inference over causal structures. *arXiv preprint*, 2021.
- Bellot, A. and Branson, K. Neural Graphical Modelling in Continuous Time: Consistency Guarantees and Algorithms. *International Conference on Learning Representations (ICLR)*, 2022.
- Bengio, E., Jain, M., Korablyov, M., Precup, D., and Bengio, Y. Flow Network based Generative Models for Non-Iterative Diverse Candidate Generation. *Advances in Neural Information Processing Systems (NeurIPS)*, 2021.
- Bengio, Y., Deleu, T., Hu, E. J., Lahlou, S., Tiwari, M., and Bengio, E. GFlowNet Foundations. *arXiv preprint 2111.09266*, 2022.
- Bergen, V., Lange, M., Peidli, S., Wolf, F. A., and Theis, F. J. Generalizing RNA velocity to transient cell states through dynamical modeling. *BioRxiv preprint 820936*, 2019.
- Chen, R. T. Q., Rubanova, Y., Bettencourt, J., and Duvenaud, D. Neural Ordinary Differential Equations. *Advances in Neural Information Processing Systems (NeurIPS)*, 2018.
- Cundy, C., Grover, A., and Ermon, S. BCD Nets: Scalable Variational Approaches for Bayesian Causal Discovery. *Advances in Neural Information Processing Systems (NeurIPS)*, 2021.
- Deleu, T., Góis, A., Emezue, C., Rankawat, M., Lacoste-Julien, S., Bauer, S., and Bengio, Y. Bayesian Structure Learning with Generative Flow Networks. *Uncertainty in Artificial Intelligence (UAI)*, 2022.
- Glymour, C., Zhang, K., and Spirtes, P. Review of Causal Discovery Methods Based on Graphical Models. *Frontiers in Genetics*, 2019.
- Granger, C. W. J. Investigating Causal Relations by Econometric Models and Cross-spectral Methods. *Econometrica: journal of the Econometric Society*, 1969.
- Hashimoto, T. B., Gifford, D. K., and Jaakkola, T. S. Learning Population-Level Diffusions with Generative Recurrent Networks. *International Conference on Machine Learning (ICML)*, 2016.
- Huguet, G., Magruder, D. S., Tong, A., Fasina, O., Kuchroo, M., Wolf, G., and Krishnaswamy, S. Manifold interpolating optimal-transport flows for trajectory inference. *Advances in Neural Information Processing Systems (NeurIPS)*, 2022a.
- Huguet, G., Tong, A., Zapatero, M. R., Wolf, G., and Krishnaswamy, S. Geodesic Sinkhorn: Optimal transport for high-dimensional datasets. *arXiv preprint 2211.00805*, 2022b.
- Kanehisa, M., Furumichi, M., Sato, Y., Ishiguro-Watanabe, M., and Tanabe, M. KEGG: Integrating viruses and cellular organisms. *Nucleic Acids Research*, 49, 2021.
- Ke, N. R., Bilaniuk, O., Goyal, A., Bauer, S., Larochelle, H., Pal, C., and Bengio, Y. Learning neural causal models from unknown interventions. *arXiv preprint 1910.01075*, 2019.
- La Manno, G., Soldatov, R., Zeisel, A., Braun, E., Hochgerner, H., Petukhov, V., Lidschreiber, K., Kastrioti, M. E., Lönnerberg, P., Furlan, A., Fan, J., Borm, L. E., Liu, Z., van Bruggen, D., Guo, J., He, X., Barker, R., Sundström, E., Castelo-Branco, G., Cramer, P., Adameyko, I., Linnarsson, S., and Kharchenko, P. V. RNA velocity of single cells. *Nature*, 560, 2018.
- Lachapelle, S., Brouillard, P., Deleu, T., and Lacoste-Julien, S. Gradient-Based Neural DAG Learning. *International Conference on Learning Representations (ICLR)*, 2020.
- Liu, Q. and Wang, D. Stein variational gradient descent: A general purpose bayesian inference algorithm. *Advances in Neural Information Processing Systems (NeurIPS)*, 2016.
- Lopez, R., Hütter, J.-C., Pritchard, J. K., and Regev, A. Large-scale differentiable causal discovery of factor graphs. *Advances in Neural Information Processing Systems (NeurIPS)*, 2022.
- Lorch, L., Rothfuss, J., Schölkopf, B., and Krause, A. DiBS: Differentiable Bayesian Structure Learning. *Advances in Neural Information Processing Systems (NeurIPS)*, 2021.
- Malkin, N., Jain, M., Bengio, E., Sun, C., and Bengio, Y. Trajectory Balance: Improved Credit Assignment in GFlowNets. *Advances in Neural Information Processing Systems (NeurIPS)*, 2022.

- Monti, R. P., Zhang, K., and Hyvärinen, A. Causal discovery with general non-linear relationships using non-linear ica. 2020.
- Mooij, J. M., Janzing, D., and Schölkopf, B. From Ordinary Differential Equations to Structural Causal Models: The deterministic case. *Uncertainty in Artificial Intelligence (UAI)*, 2013.
- Mooij, J. M., Magliacane, S., and Claassen, T. Joint causal inference from multiple contexts. *The Journal of Machine Learning Research (JMLR)*, 21, 2020.
- Pearl, J. *Causality*. Caimbridge University Press, second edition, 2009.
- Peters, J., Janzing, D., and Schölkopf, B. *Elements of causal inference: foundations and learning algorithms*. The MIT Press, 2017.
- Peters, J., Bauer, S., and Pfister, N. Causal models for dynamical systems. *Probabilistic and Causal Inference: The Works of Judea Pearl*, 2022.
- Qiu, X., Zhang, Y., Martin-Rufino, J. D., Weng, C., Hosseinzadeh, S., Yang, D., Pogson, A. N., Hein, M. Y., Hoi (Joseph) Min, K., Wang, L., Grody, E. I., Shurtleff, M. J., Yuan, R., Xu, S., Ma, Y., Replogle, J. M., Lander, E. S., Darmanis, S., Bahar, I., Sankaran, V. G., Xing, J., and Weissman, J. S. Mapping transcriptomic vector fields of single cells. *Cell*, 185, 2022.
- Riba, A., Oravec, A., Durik, M., Jiménez, S., Alunni, V., Cerciati, M., Jung, M., Keime, C., Keyes, W. M., and Molina, N. Cell cycle gene regulation dynamics revealed by RNA velocity and deep-learning. *Nature Communications*, 13, 2022.
- Saelens, W., Cannoodt, R., Todorov, H., and Saeys, Y. A comparison of single-cell trajectory inference methods. *Nature Biotechnology*, 37, 2019.
- Schiebinger, G., Shu, J., Tabaka, M., Cleary, B., Subramanian, V., Solomon, A., Gould, J., Liu, S., Lin, S., Berube, P., Lee, L., Chen, J., Brumbaugh, J., Rigollet, P., Hochedlinger, K., Jaenisch, R., Regev, A., and Lander, E. S. Optimal-Transport Analysis of Single-Cell Gene Expression Identifies Developmental Trajectories in Reprogramming. *Cell*, 176, 2019.
- Spirtes, P. and Glymour, C. An algorithm for fast recovery of sparse causal graphs. *Social Science Computer Review*, 9, 1991.
- Tank, A., Covert, I., Foti, N., Shojaie, A., and Fox, E. Neural Granger Causality. *IEEE Transactions on Pattern Analysis and Machine Intelligence*, 2021.
- Tong, A., Huang, J., Wolf, G., van Dijk, D., and Krishnaswamy, S. TrajectoryNet: A Dynamic Optimal Transport Network for Modeling Cellular Dynamics. *International Conference on Machine Learning (ICML)*, 2020.
- Zheng, X., Aragam, B., Ravikumar, P., and Xing, E. P. DAGs with NO TEARS: Continuous Optimization for Structure Learning. *Advances in Neural Information Processing Systems (NeurIPS)*, 2018.

Supplementary Material

A. Proof of Proposition 1

Proposition 1 calculates the number of admissible structure graphs for a linear ODE system with correlated variables. We will first show the general case this is $\prod_{i \in d} (2^{m_i} - 1)^{\mathcal{G}_i^1}$, then analyze the case of an L^0 penalty on the edges of G , which reduces the size of the set of admissible graphs to $\prod_i (m_i)^{\mathcal{G}_i^1}$.

Proof. Consider an identifiable linear system $\frac{dx}{dt} = Ax$ where we directly observe $(x, \frac{dx}{dt})$ with \mathcal{G}^* identifiable. Then the system with $m = \mathbf{1}^d$ has exactly one admissible graph by definition. For each node, we analyze its set of child nodes in \mathcal{G} , i.e. $c(u) = \{v \in \mathcal{V} \text{ s.t. } u \rightarrow v \in \mathcal{G}\}$. For an identifiable system, each child v must have an incoming edge from its parent.

Next, we consider the process of adding a correlated variable, i.e. consider the situation of w.l.o.g. consider $m = (s, 1, 1, \dots, 1)$ for some $s > 1$. Then for each child of $c_j(v_1)$, there are now s possible parents. This has multiplied the number of possible graphs by $2^s - 1$. Since each element of m is independent, this leads to the first statement, i.e. $|\mathcal{G}'| = \prod_{i \in d} (2^{m_i} - 1)^{\mathcal{G}_i^1}$.

Under an L^0 penalty, then we constrain the possible graphs to s different graphs, where each child node picks exactly one of the s possible parents. This leads to the second statement, $|\mathcal{G}'| = \prod_i (m_i)^{\mathcal{G}_i^1}$ \square

B. Experimental Details

B.1. Single Cell Dataset Preprocessing

We start with the processed data from (Riba et al., 2022). We first filter it applying steps from the ScVelo tutorial. We then sub-select the genes of interest and use the “Ms” and “velocity” layers, which we normalize to mean zero standard deviation one for the states and scale the dx with the same parameters.

B.2. Hyper-parameters for Baselines

For both DynBCD and DynDiBS we use $k = d$ across datasets. Since DynDiBS is an ensemble based method, we use 1024 samples for the linear and non-linear synthetic systems and 1000 samples for the cellular system (both training and evaluation). Since DynBCD is a variational approach and doesn’t require parallelized model ensembles, we use a large quantity of samples for training and evaluation. In the case of the cellular system, since there is a significantly smaller quantity of admissible graphs, we use less samples for DynBCD. We use graph sparsity regularization denoted by λ_0 and a temperature parameter T that scales the mag-

nitude of the likelihood (e.g. $\frac{1}{T^2} \text{MSE}(dx, \widehat{dx})$). In Table 4 and Table 5 we outline the hyper-parameters we found to yield the most competitive results. We use grid search to tune DynBCD and DynDiBS. All baselines are trained for 1000 epochs.

Table 4. Hyper-parameters for DynBCD. We define learning rate as ϵ .

Linear System					
Model	ϵ	λ_0	T	α	samples
ℓ -DynBCD	0.0001	0.001	0.01	0.1	5000
h -DynBCD	0.0001	0.0025	0.01	2	2000

Non-linear System					
Model	ϵ	λ_0	T	α	samples
ℓ -DynBCD	0.00005	0.001	0.01	2	5000
h -DynBCD	0.0001	0.001	0.01	1	2000

Cellular System					
Model	ϵ	λ_0	T	α	samples
ℓ -DynBCD	0.0001	0.001	0.05	0.05	1000
h -DynBCD	0.00001	0.0005	0.1	2	1000

Table 5. Hyper-parameters for DynDiBS. We define learning rate as ϵ .

Linear System					
Model	ϵ	λ_0	T	α	γ
ℓ -DynDiBS	0.0025	500	0.01	0.0001	3000
h -DynDiBS	0.0001	3	0.01	0.0001	10000

Non-linear System					
Model	ϵ	λ_0	T	α	γ
ℓ -DynDiBS	0.001	10	0.01	0.0001	3000
h -DynDiBS	0.0001	0.1	0.01	0.0001	10000

Cellular System					
Model	ϵ	λ_0	T	α	γ
ℓ -DynDiBS	0.0025	1	0.05	0.0001	3000
h -DynDiBS	0.00001	0.1	0.01	0.01	3000

We note that when evaluation on validation and test data for Bayes-SHD and AUC metrics, we hard threshold $P_{\alpha_t}(G|Z)$. We find that through training this the final α_t is typically small enough in magnitude such that $P_{\alpha_t}(G|Z)$ does not yield a full threshold of Z . To this end, we select large α_t when computing the KL metric to mimic hard threshold behaviour as experienced during training. We use $\alpha_t = 1 \times 10^4$ for DynBCD and $\alpha_t = 1 \times 10^8$ for DynDiBS methods, respectively. In DynDiBS The parameter γ helps control separation of particles Z during training. In general, we found DynBCD and DynDiBS baselines challenging to train and find hyper-parameter settings with good performance. In part, we believe this is due to the numerous

hyper-parameters required to set as well as the general difficulty of the objective.

B.3. Neural Network Architectures and Hyper-parameters

We parameterize $P_F(s_i|s_{i-1}; \psi)$ and h_ϕ with MLP architectures. $P_F(s_i|s_{i-1}; \psi)$ takes the current state as input and firsts computes common representations using a 3 layer MLP. Then a 2 layer MLP with a softmax output activation takes the representations as input and outputs a distribution over possible actions. The latter MLP is used to parameterize one head for each distribution $P_F(s_i|s_{i-1}; \psi)$. We use a hidden unit dimension of 128 and leaky rectified linear unit (Leaky ReLU) activation functions for the $P_F(s_i|s_{i-1}; \psi)$ MLP architecture. We use a uniform backward policy for $P_B(s_{i-1}|s_i; \psi)$. To parameterize h_ϕ , we use a 3 layer MLP with hidden layer dimensions of $\{64, 64, 64\}$ and exponential linear unit activations (ELU). We consider two parametrizations for f_θ : single linear parameters, i.e $dx = \theta x$, and a single hidden layer neural network $dx = f_\theta(x)$. We use these parametrizations to model linear and non-linear node-wise parent-child structural equations, where $x \in \mathbb{R}^d$ are the node-wise input observations.

B.4. Hyper-parameters for DynGFN

DynGFN requires setting a variety of hyper-parameters that lead to different trade offs in model performance. In particular, λ_0 (sparsity encouragement for identified graphs), a temperature parameter T that scales the magnitude of the reward likelihood (e.g. $\frac{1}{T^2} \text{MSE}(dx, \widehat{dx})$), learning rate ϵ , softmax tempering c (we always use a cosine schedule for c , with a discrete period of 5 epochs), and number of training epochs. In our experiments we use grid search to select hyper-parameter values that lead to competitive performance (this pertains to ℓ -DynGFN and h -DynGFN models). We outline the best performing hyper-parameters for each respective model in Table 6. Due to computational limits, we use less training sample than evaluation sampled for DynGFN. We train DynGFN for 1000 epochs.

B.5. Implementation Details

Our model is implemented in Pytorch and Pytorch Lightning and is available at <https://github.com/lazaratan/dyn-gfn>. Models were trained on a heterogeneous mix of HPC clusters for a total of 1,000 GPU hours primarily on NVIDIA RTX8000 GPUs.

Table 6. Hyper-parameters for DynGFN. We define learning rate as ϵ , m_{train} as number of training samples, and m_{eval} the number of evaluation samples.

Linear System					
Model	ϵ	λ_0	T	m_{train}	m_{eval}
ℓ -DynGFN	0.0001	100	0.01	1024	5000
h -DynGFN	0.00001	400	0.005	256	3000

Non-linear System					
Model	ϵ	λ_0	T	m_{train}	m_{eval}
ℓ -DynGFN	0.0001	150	0.01	1024	5000
h -DynGFN	0.00001	300	0.005	256	3000

Cellular System					
Model	ϵ	λ_0	T	m_{train}	m_{eval}
ℓ -DynGFN	0.00005	45	0.01	1024	1000
h -DynGFN	0.0001	10	0.1	1024	1000